IMPURITY EFFECTS ON ACTIVATION ENERGY, STRUCTURE AND PHYSICAL PROPERTIES OF YBCO SUPERCONDUCTOR

Murat ÖZABACI

Scientific and Technological Research Center, Inonu University, Malatya, TURKEY

ABSTRACT. The influence of separately added 0.3 wt%, CdO, Bi_2O_3, BeO and SiO_2 on the phase formation, microstructure, magnetic and transport properties of $Y_1Ba_2Cu_3O_{7-\delta}$ (Y-123 or YBCO) fabricated by conventional solid state reaction method has been analyzed. The results reveal a very low solubility limit for bismuth and silicon in the Y-123 phase, leading to precipitation phases located within intergranular regions. BeO addition suppresses the granular nature of the structure by probably incorporating into the host matrix. CdO does not have a remarkable effect both on structural and superconducting properties of the Y-123 at this doping ratio. Attractive infield transition behavior was obtained in the Bi_2O_3 added sample with a narrower transition width and an increase of transition temperatures approximately 1 K. The activation energy (U_0), a potential energy barrier to prevent flux flow, of the samples was estimated by taking into account Arrhenius law. The best U_0 value was computed to be 1.11 eV belonging to the Bi_2O_3 added sample which implies the contribution of 3-5 μm sized Bi containing precipitation regions on the flux pinning capability of the Y-123.

1. INTRODUCTION

$Y_1Ba_2Cu_3O_{7-\delta}$ (Y-123) superconductors are considered as one of the most promising candidates for engineering applications of bulk superconductors [1,2]. Examples of such applications include magnetic bearings, flywheel energy storage systems, trapped flux magnets and levitation, requiring large-grain materials in various shapes [3,4]. However, there are still some limitations for technological applications of Y-123 caused by the rapid decay of the critical current density (J_c) in a magnetic field, which is strictly related with the lack of effective flux pinning centers and the magnitude of the activation energies. Many attempts on applications of Y-123 have

showed that the exposure of high magnetic fields and temperatures causes flux creep, which is responsible for energy dissipation and subsequent loss of superconductivity [5-8].

In order to introduce artificial pinning centers and enhance the flux pinning strength further, various approaches have been adopted previously including substitution of constitutional elements and creating defects through electron, x-ray, neutron or heavy ion irradiation [9-12]. Among these methods, chemical doping is considered to be the most effective way of enhancing J_c, because of the relative simplicity of fabrication, low-cost and flexibility. The literature contains many papers concerning the chemical doping with additions and substitutions of graphene, Ca, Zn, Sr, Ti, La, Al, Gd, Ag, Ce, Co, Fe, Sb, Nb, C, Ni, Yb, Cu, Au, Lu, Pr, Sm and Ba, as examples [13-23].

The aim of this work is to comparatively investigate the effect of 0.3 wt%, CdO, Bi_2O_3, BeO and SiO_2 additions on the phase formation, microstructure, electrical and magnetic properties of the bulk $Y_1Ba_2Cu_3O_{7-\delta}$ superconductors. Activation energy of flux motion or pinning potential (U_0) and upper critical magnetic field (H_{c2}) values are deduced from the magneto-resistivity curves by means of thermally activated flux flow (TAFF) theory [24, 25]. It has been found that four different additions give rise to various influences easily detectable both on microstructure and critical superconducting parameters of the Y-123.

The literature contains a number of papers concerning the additions and substitutions of CdO, Bi_2O_3, BeO and SiO_2 compositions to the various formations and stoichiometries of YBCO [26-29]. Our principal motivation in studying these additions is to elucidate the effects of the dopants having different atomic diameters and metallic character on the structural, electrical and magnetic properties of the Y-123 fabricated under the same conditions and to optimize the size and density of pinning centers. One can see that our results are generally consistent with the previously published data on YBCO. Acetate-tartrate and biopolymer-mediated sol-gel techniques and melt-texturing are frequently applied synthesizing routes in these studies. $Y_1Ba_2Cu_4O_8$ elemental composition is the one used as an alternative of the $Y_1Ba_2Cu_3O_{7-\delta}$ to investigate the variations of superconductivity in one of these researches [26].

2. EXPERIMENTAL

The $Y_1Ba_2Cu_3O_{7-\delta}$ (Y-123 or YBCO) samples with additions of 0.3 wt%, CdO (Sigma-Aldrich, 99.5%), Bi_2O_3 (Sigma-Aldrich, 99.5%), BeO (Alfa Aesar, 99%) and SiO_2 (Alfa Aesar, 99.5%) were prepared by a solid state reaction method.

Stoichiometric proportions of thoroughly mixed Y_2O_3 (Reacton, 99.9%), $BaCO_3$ (Aldrich, 99+%), CuO (Alfa Aesar, 99.7%) and separately added CdO, Bi_2O_3, BeO and SiO_2 were calcinated for 24 h at 800 °C and 850 °C with two intermediate grindings. After calcination, the powders were pressed into pellets of 2 mm thickness and 13 mm diameter at 400 MPa. The final pellets were annealed at 980 °C for 24 h and then cooled to 500 °C where these were kept for 4 h, in a flowing oxygen atmosphere, before slowly cooling to room temperature.

All samples were characterized by X-ray powder diffraction (XRD) using a Rigaku Miniflex 600 diffractometer with Cu-Kα (40 kV, 15 mA, λ=1.54050 Å) radiation over the range 2θ=10-80° at room temperature at a scan rate of 3°/min. The microstructure and elemental distribution of the samples were investigated using LEO EVO-40 scanning electron microscope (SEM) attached with a Bruker energy dispersive X-ray spectrometer (EDX) with an accelerating voltage of 20 kV in the secondary electron image mode. Transport and DC magnetic measurements (*R-T, MR-T, M-T* and *M-H*) were performed with Quantum Design Physical Property Measurement System (PPMS), 9 T. The electrical resistivity measurements, from 30 to 150 K, (*R-T*) were conducted by means of conventional four-probe configuraton in self-field and under DC magnetic fields of 2, 4, 6 and 8 T with an applied current of 1 mA AC (17 Hz). Superconducting transition temperatures (T_c), which were used for the calculation of the U_0 and H_{c2}, were derived from the magneto-resistivity (*MR-T*) curves. The magnetic hysteresis cycles (*M-H*) were measured at 10, 20 and 30 K up to 8 T. The transition behavior of the samples were also evaluated through magnetization-temperature (*M-T*) measurements performed in both field-cooled (FC) and zero-field-cooled (ZFC) modes under 100 Oe.

3. RESULTS AND DISCUSSION

Figure 1 shows the powder X-ray diffraction patterns of the both undoped and slightly doped YBCO samples together with corresponding (*hkl*) Miller indices. It is evident in the figure that all the main XRD peaks of the samples belong to orthorhombic phase of Y-123. The Miller indices show the characteristic polycrystalline structure of the Y-123 compound without any alignment, as expected. The absence of secondary phases in the pattern, such as Y_2O_3, $BaCO_3$, $BaCuO_2$ and Y_2BaCuO_5 confirms that the annealing procedure in the flowing oxygen atmosphere is adequate to obtain highly pure samples. In all the obtained patterns, it could not be observed an appreciable shift of the peaks upon CdO, Bi_2O_3, BeO and SiO_2 additions, which might be ascribed to the minor amount of inclusions in the samples. It should be noted that it is hard to detect small concentrations in x-ray measurements. The relative intensity, sharpness and width of the peaks also remain

almost unchanged irrespective of the added compositions. However, comparative analysis of the XRD patterns reveals a weakness in the intensity and sharpness of the peaks of the BeO added sample, indicative of a decrement of the crystal quality.

Surface morphologies of the samples are shown in Figures 2a to 2e. All of the samples fabricated, except for the BeO-doped one, show clear characteristic granular structure of the Y-123. The micrographs exhibit a layered growth nature of the grains in some regions. The grains are disordered with irregular shapes, as expected. Spherical plate-like grains along with rectangular-like grains can also be easily identified in the samples. There is also a small amount of circular pores between the closely packed grains. CdO addition does not lead to a distinguishable change on the surface morphology of the sample, while Bi_2O_3 addition gives rise to some heterogeneous precipitation regions. It is easily noticed in the Figure 2d that the introduction of BeO to the Y-123 disrupts the granular structure of the Y-123 and the grains become more joined due to the reduction of intergranular space. In this way, the interconnection regions between the grains partially vanish, which supports the associated XRD result. It is evaluated that the Be atoms, because of their small atomic diameter, easily incorporate into the host matrix and partially prevents the formation of the Y-123 phase. SiO_2 addition gives rise to a similar effect on the structure with that of Bi_2O_3 addition by leading to formation of macroscale non-superconducting precipitates at some grain boundaries. However, it is observed that the diameter of these regions increases from the 3-5 µm, in the Bi_2O_3-added sample, to the 8-12 µm, in the SiO_2-added one. This shows that solid solubilities of the Bi and Si atoms in the Y-123 are even lower than the 0.3 wt%, which may be attributed to their large atomic diameter along with low metallic character.

Analysis of the elemental compositions on the main matrix based on the EDX spectra shows that in all the samples the elemental ratios correspond to the nominal chemical formula of the Y-123. The signal stemming from the Cd could not be detected on the EDX spectra, which is attributed to the amount of doping that is below EDX detection limit and uniform distribution of the Cd atoms over the grains. Be could not be quantified in the EDX software because of the limitations of the EDX instrument. The precipitation regions observed on the Bi_2O_3-added sample include only Bi and O atoms, while on the SiO_2-added one, consist of both Si and Ba in addition to the O (see Figures 3a-3d) with a stoichiometry appropriate to the $BaSiO_3$. This shows that Si and Ba atoms positively react with each other to form a new phase. From this observation, we can conclude that the presence of SiO_2 in the structure arises a small degree of Y-Ba disorder in the crystal and liberates some Ba from the Y-123 phase.

Figure 4 displays the temperature behavior of the magnetization for the samples both at field-cooled (FC) and zero-field-cooled (ZFC) modes. The diamagnetic transition temperatures, T_c^{mag}, were found to be between 89.8-90.3 K and 90.9-91.5 K in FC and ZFC modes, respectively. This shows that introduction of various compositions does not have a significant influence on T_c^{mag} for the 0.3 wt% doping amount in Y-123. However, saturation magnetization levels show differences depending on added compositions and measurement conditions. It is worth mentioning that the strongest diamagnetism was obtained in the CdO added sample, while the weakest diamagnetism in the BeO added sample in the FC mode. This is in good agreement with the expected behavior from the above-mentioned XRD and SEM results, i.e., as the crystal quality decreases, diamagnetic shielding attenuates.

The magnetic hysteresis loops (*M–H*) for the studied samples were obtained in the applied field range of ±8 Tesla in the temperatures of the 10, 20, and 30 K, see Figures 5a-5c. All samples show similar symmetrical behavior which is a characteristic of high temperature superconductors (HTSCs). The difference of magnetic moments between descending and ascending field branches of the magnetic hysteresis loops is partially proportional with the magnitude of the critical current densities (J_c^{mag}) of the superconducting samples. Since this difference is larger for the BeO and SiO_2 added samples, a higher J_c^{mag} is expected for these samples, compared to that of undoped one. This enlargement may be caused by the enhancement of pinning capability of the samples through a possible increase in extended point-like defects and crystal distortions, as partially observed in SEM and XRD measurements. It seems that the addition of Bi_2O_3 has also the potential to enhance the J_c^{mag} because of the enlargement of the corresponding *M-H* loop, while for the CdO addition, there is no evidence of the improvement of the J_c^{mag}.

The temperature-dependent resistivity (*MR-T*) measurements of the samples were performed under applied magnetic fields of 0, 2, 4, 6 and 8 T. Representative measurements and T_cs deduced from the *MR-T* curves are shown in Figures 6a-6c and Table 1, respectively. The figures show that the transition takes place within a narrow temperature range, i.e. $\Delta T \leq 4$ K, implying the high degree of inter-grain connectivity and compact crystal structure of the samples. All samples show metallic behavior in the normal state because of the almost linear decrease of the resistivity down to onset of superconductivity (T_c^{onset}) with decreasing temperature. The figures show that zero resistance state temperature (T_c^{zero}) of the samples seriously shifts to lower temperatures with increasing magnetic field while T_c^{onset} values are weakly affected from the increased magnetic field. The decrease of the T_c^{zero} values is originated by the appearance of resistive tails on the lower temperature end of *R-T* curves. The tailing behavior is known to be correlated with the high thermal energy

of vortices and flux flow by Lorentz force which is known as TAFF [30,31]. The disorders in the percolation path owing to the randomly oriented grains of polycrystalline samples also contribute this behavior.

The presence of the inclusions does not have a serious influence on the T_cs and ΔTs in the absence of field. The most significant effect of increasing applied magnetic field is observed on the BeO and SiO$_2$ added samples with an increase of ΔT from 14.1 K, for the undoped sample, to the ΔT=20.2 and 18.8 K for the BeO and SiO$_2$ added samples, respectively. These results are in good agreement with the results obtained by XRD and SEM analysis. It is evaluated that the additions of BeO and SiO$_2$ distort the atomic structural arrangement and phase formation of Y-123 through two different mechanisms: Be atoms incorporate into the crystal structure and create considerable distortions in the lattice and Si atoms react with the Ba atoms to form a new non-superconducting secondary phase. In this way, optimal carrier concentration of the structure is being damaged and thus the emergence of zero resistance state shifts to lower temperatures. On the other hand, we notice an increase (~1 K) in T_cs of the Bi$_2$O$_3$ added sample which could be ascribed to the formation of precipitation regions. Since the added Bi$_2$O$_3$ is not completely dissolved in Y-123, as observed in SEM images, it is suggested that Bi atoms do not substitute the major components of the Y-123 and create conductive paths by adhering to grain boundary forming weak links. This behavior can improve inter-grain connectivity and allows for higher oxygen coordination by leading optimal porosity.

We have calculated the activation energy, U_0, of the superconducting samples by using the well-known Arrhenius equation, $\rho\,(B,T) = \rho_0 \exp(-U_0/k_B T)$, where ρ_0 is the pre-exponential factor, k_B is Boltzmann constant and U_0 is the activation energy, which is a potential energy barrier to keep the magnetic flux in pinning center and gives the magnitude of the effective pinning energy [32, 33]. Figures 7a through 7e show Arrhenius plots, Inρ/ρ_0 versus $1/T$, of the studied samples. In the figure, the activation energies are extracted from the slope of linear part of the low resistivity region, which are indicated by the linear fitting lines for the undoped sample in Figure 7a as representative of the series. It is clear in the figure that the flux creep activation energy is higher for Bi$_2$O$_3$ added sample. This increase in U_0 shows that the flux lines are better pinned in the Bi$_2$O$_3$ added sample which, in turn, would improve its superconducting behavior in a magnetic environment. Additions of BeO and SiO$_2$ result in a decrease of flux pinning while addition of CdO does not give rise to a significant change in comparing with pure Y-123 as demonstrated in the Figure 7f.

For the estimation of temperature dependence of the upper critical magnetic field, $H_{c2}(0)$, of the samples, simplified Werthamer-Helfand-Hohenberg (WHH) model

was used, where $H_{c2}(0)$ is formulated as $H_{c2}(0) = -0.693T_c \left(\frac{dH_{c2}}{dT}\right)_{T_c}$ and dH_{c2}/dT is the slope of $H_{c2}(T)$ near T_c and derived from the plots given in Figure 6 [34]. Here, we used the T_c^{midpoint} data, where the resistivity becomes 50% of its normal state value (ρ_n), given in Table 1 in the equation. The calculated $H_{c2}(0)$ values are 48.2, 45.7, 45.8, 47.1 and 45.4 T for the pure, CdO, Bi$_2$O$_3$, BeO and SiO$_2$ added samples, respectively, which are below the single crystal Y-123 counterparts and comparable with the polycrystalline samples reported in different studies [35-37]. It is concluded from these results that the $H_{c2}(0)$ values of polycrystalline Y123 samples are weakly affected from the studied amounts of doping.

4. CONCLUSIONS

The effects promoted by additions of 0.3 wt% CdO, Bi$_2$O$_3$, BeO and SiO$_2$ on phase formation, crystal structure, magnetic and electrical properties of the polycrystalline Y-123 samples have been studied. The XRD results show single phase orthorhombic Y-123 for the whole range of impurities. It has been found that BeO inclusions slightly degrade the intensity and sharpness of the XRD peaks. SEM/EDX investigations reveal that BeO addition causes a disruption on the granular structure. CdO addition does not lead to a remarkable change on the surface morphology of the Y-123, while SiO$_2$ and Bi$_2$O$_3$ additions form some heterogeneous precipitation phases within the intergranular regions. It has been observed that Bi atoms does not react with the constitutional elements in contrast to the Si atoms, which generate a phase conforming well to the BaSiO$_3$ stoichiometry on the precipitation regions. T_c^{mag} values are not seriously affected from the additions and found to be around 91 K. Magneto-resistivity measurements show that BeO and SiO$_2$ added samples are more sensitive to the external magnetic field than the other samples, as a probable consequence of the modification of the hole carrier concentration from the optimal values and the disorder in the CuO$_2$ planes. CdO was found to be completely dissolved in the matrix and no evidence of variation in the magnetic and electrical properties of the Y-123 was obtained. It is concluded that the Bi$_2$O$_3$ addition, among the studied compositions, produces the most favorable superconducting performance in regard to the transition behavior under magnetic field and the activation energy. Induction in overall oxygen content by leading optimal porosity and depression of grain boundary effect are considered to be the possible mechanisms occurring in the Bi$_2$O$_3$ added sample responsible for promising performance in high field applications.

TABLE 1. Superconducting transition temperatures (in kelvin) of the samples derived from both *MR-T* and *M-T* measurements. $T_c^{midpoint}$ values were inferred from the peak points of the $d\rho/dT$ curves.

| Composition	M-T T_c^{mag} FC	M-T T_c^{mag} ZFC	MR-T 0 T T_c^{onset}	MR-T 0 T T_c^{zero}	MR-T 0 T ΔT	MR-T 0 T T_c^{midp}	MR-T 4 T T_c^{onset}	MR-T 4 T T_c^{zero}	MR-T 4 T ΔT	MR-T 4 T T_c^{midpo}	MR-T 8 T T_c^{onset}	MR-T 8 T T_c^{zero}	MR-T 8 T ΔT	MR-T 8 T $T_c^{midpoint}$
Undoped	89.8	90.9	91.0	87.0	4.0	90.4	90.0	77.8	12.2	87.2	89.0	74.9	14.1	85.7
CdO	89.8	91.0	91.0	87.0	4.0	90.3	89.8	77.5	12.3	86.8	89.1	74.4	14.7	85.9
Bi₂O₃	90.1	91.3	91.3	88.0	3.3	90.2	90.2	79.1	11.1	87.8	90.5	75.8	14.7	86.4
BeO	90.3	91.3	91.6	88.0	3.6	90.7	92.1	75.8	16.3	88.6	92.2	72.0	20.2	87.5
SiO₂	90.2	91.5	91.3	87.7	3.6	90.1	91.0	76.0	15.0	87.8	91.3	72.5	18.8	86.7
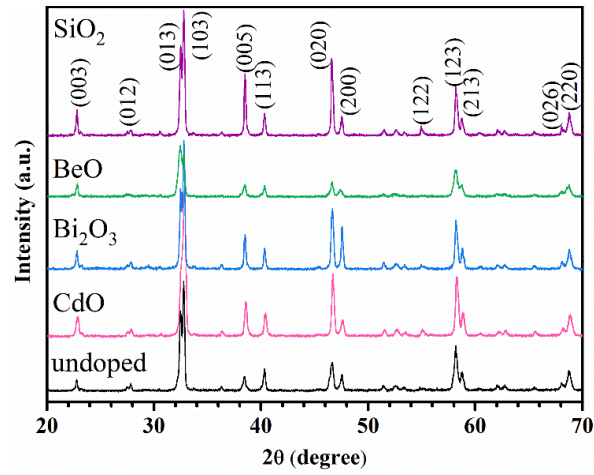
FIGURE 1. Powder XRD patterns of the pure and 0.30 wt.% added $Y_1Ba_2Cu_3O_{7-\delta}$ samples.
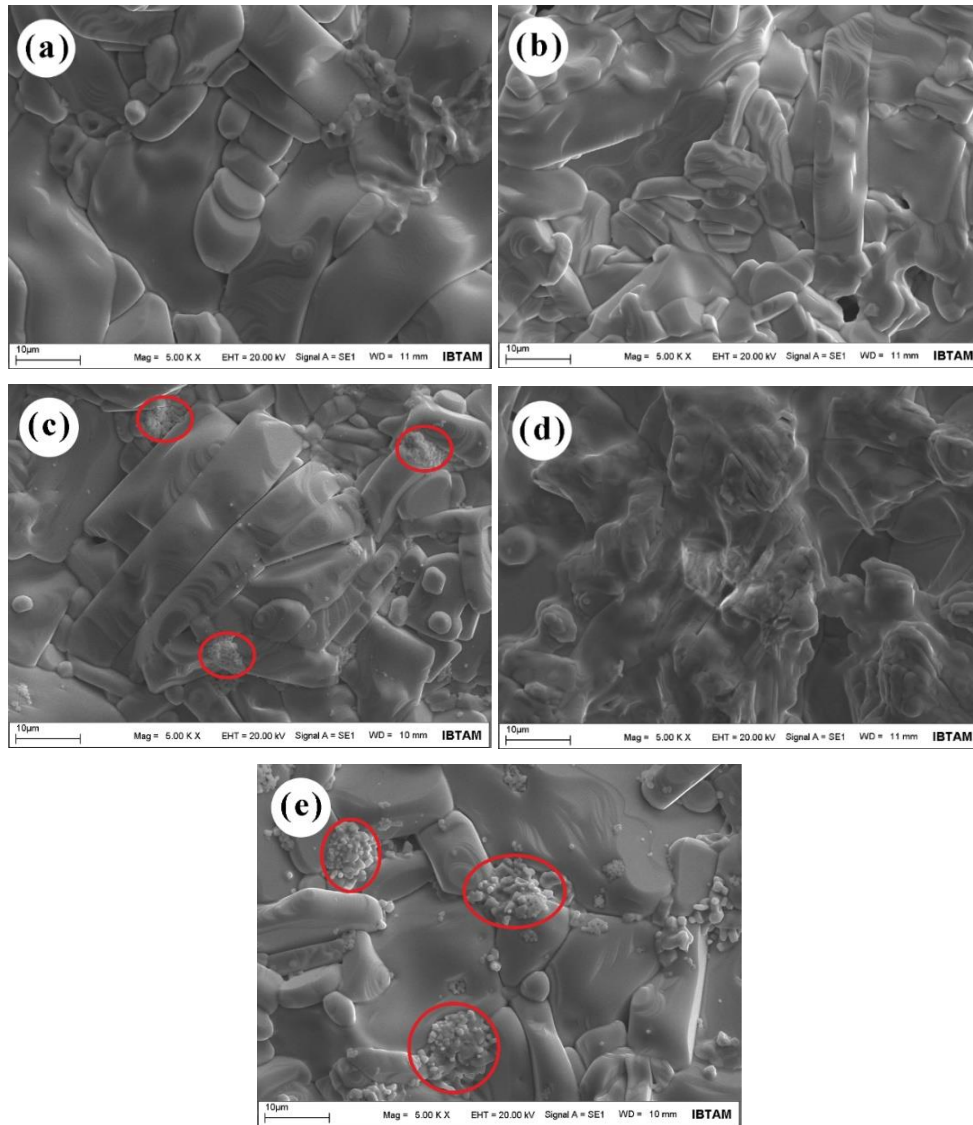
FIGURE 2. SEM images of the $Y_1Ba_2Cu_3O_{7-\delta}$ bulk samples at x5000 magnification and a scale of 10 µm with 0.30 wt. % additives: a) Undoped, b) CdO, c) Bi_2O_3, Bi-precipitation regions are enclosed by the red ellipses, d) BeO and e) SiO_2, Ba and Si rich heterogeneous regions are indicated by the red ellipses.
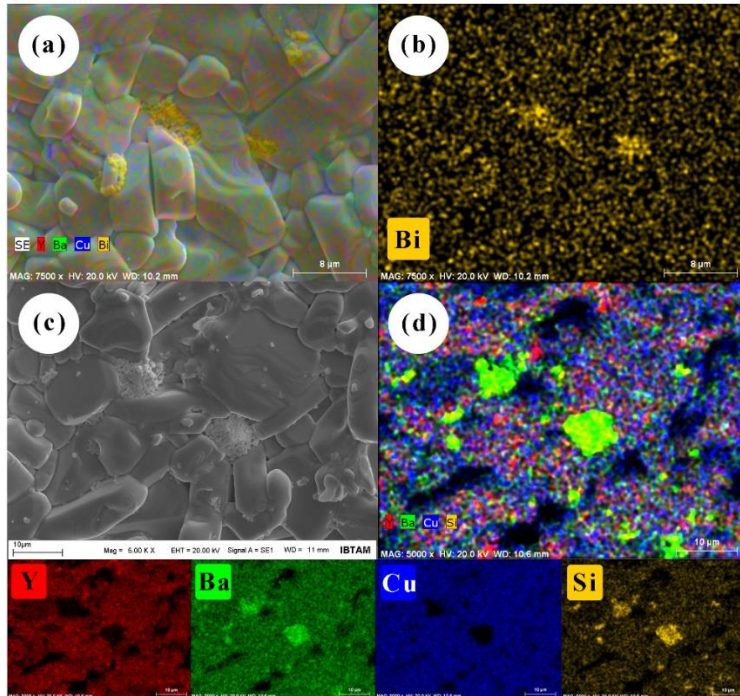
FIGURE 3. EDX elemental mapping and SEM images of the samples having heterogeneous precipitation regions: a-b) Bi_2O_3 added $Y_1Ba_2Cu_3O_{7-\delta}$, c-d) SiO_2 added $Y_1Ba_2Cu_3O_{7-\delta}$. Color images at the bottom show the elemental distribution of the Si-doped sample for each element in the structure.
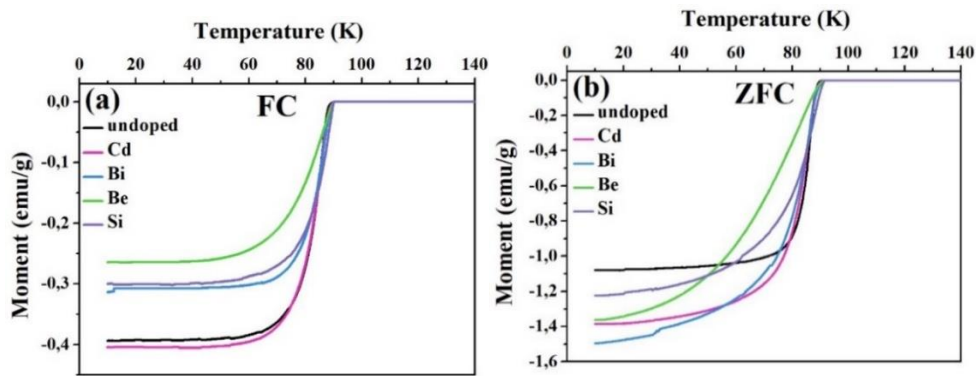

FIGURE 4. Low-field magnetization vs. temperature curves of the studied samples in a) FC and b) ZFC modes.
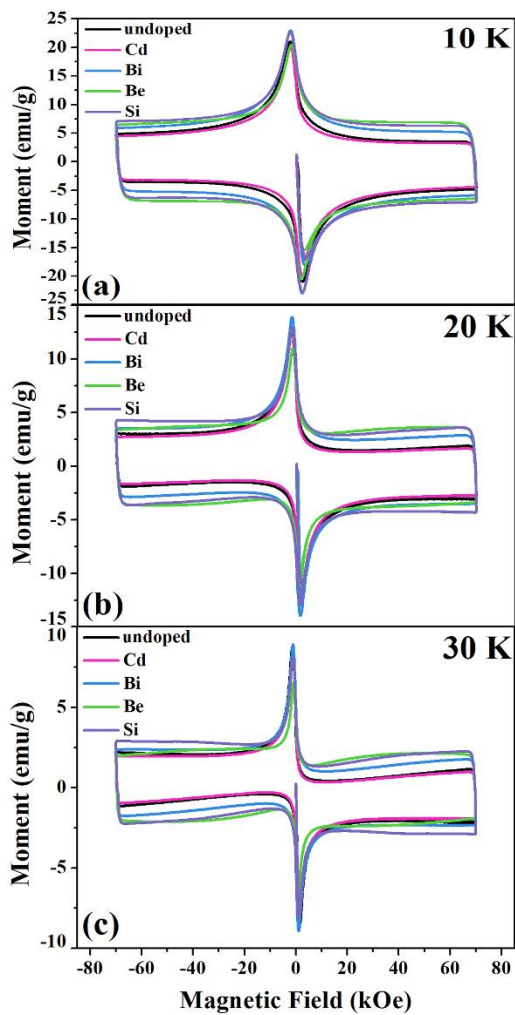
FIGURE 5. Magnetization vs. magnetic field curves of the studied samples at a) 10 K, b) 20 K and c) 30 K.
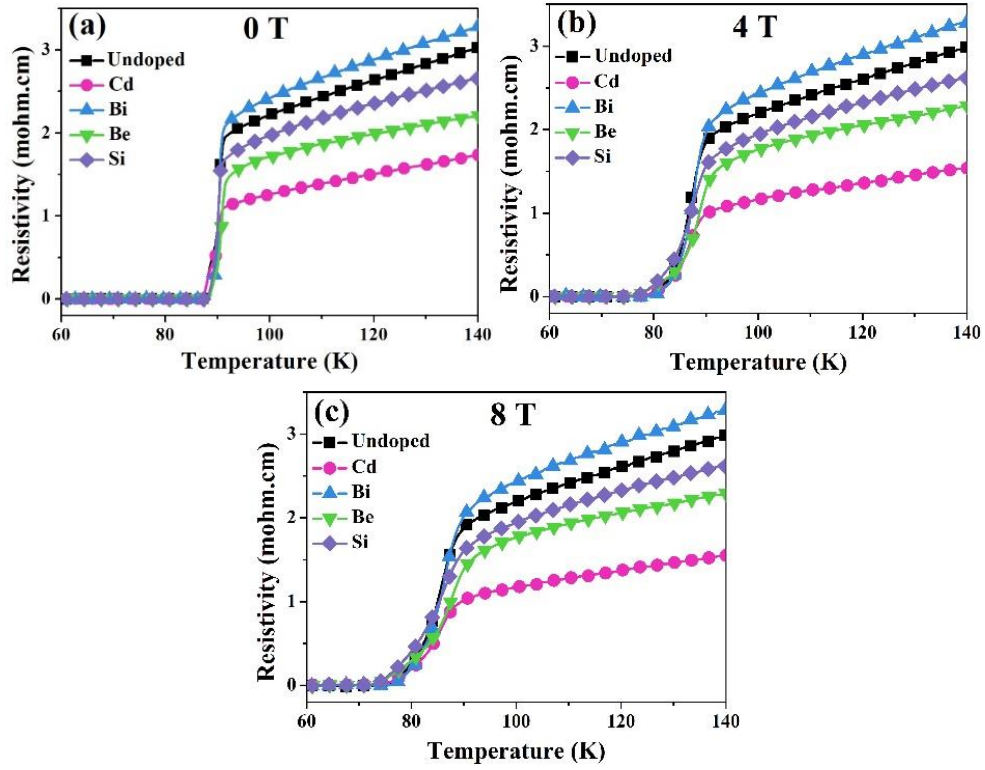
FIGURE 6. Effect of applied magnetic fields, a) 0 T, b) 4 T and c) 8 T, on the resistivity-temperature curves of the samples.
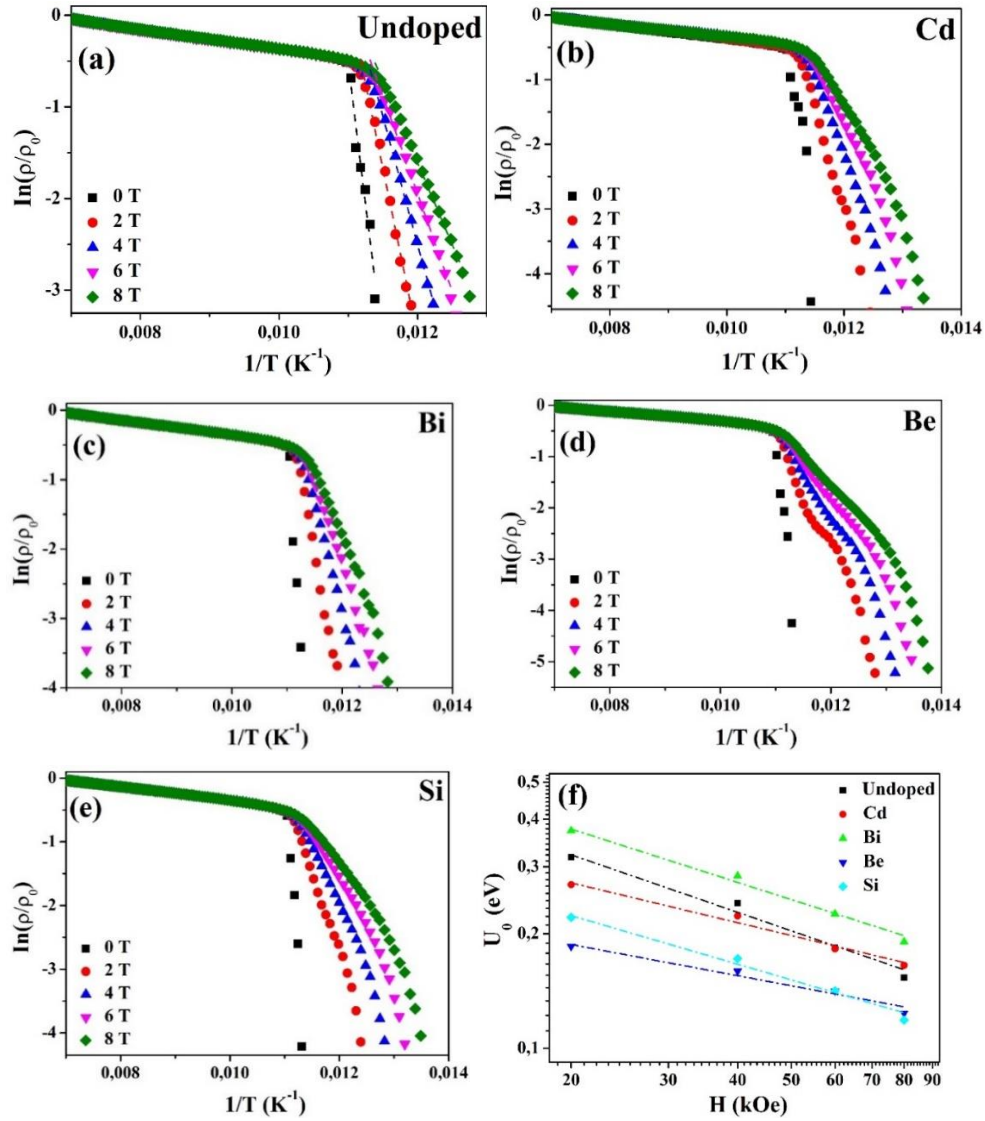
FIGURE 7. a-e) Arrhenius plots of the normalized electrical resistivity of the samples with different additives, f) magnetic field dependent activation energy of the samples. The dashed lines in (a) represent the linear fittings in the low resistivity region used to calculate activation energies. The dash-dotted lines connecting the points in (f) are guides to the eye.

Declaration of Competing Interest The author declares that there is no conflict of interest.

REFERENCES

[1] Tomita, M., Murakami, M., High-temperature superconductor bulk magnets that can trap magnetic fields of over 17 T at 29 K, *Nature*, 421 (2003), 517-520. https://doi.org/10.1038/nature01350

[2] Muralidhar, M., Superconductivity: Applications Today and Tomorrow, NOVA Science, New York, 2015.

[3] Campbell, A.M., Cardwell, D.A., Bulk high temperature superconductors for magnet applications, *Cryogenics*, 37 (10) (1997), 567-575. https://doi.org/10.1016/S0011-2275(97)00068-4

[4] Hellman, F., Gyorgy, E.M., Johnson, D.W., Wang, J.R., Sherwood, R.C., Levitation of a magnet over a flat type II superconductor, *J. Appl. Phys.*, 63 (1988), 447-450. https://doi.org/10.1063/1.340262

[5] Huang, J., Li, L., Wang, X., Qi, Z., Sebastian, M.A.P., Haugan, T.J., Wang, H., Enhanced flux pinning properties of YBCO thin films with various pinning landscapes, *IEEE T. Appl. Supercon.*, 27 (4) (2017), 8000305. https://doi: 10.1109/TASC.2016.2637315

[6] Kim, C.J., Yoon, J.S., No, K., Han, S.C., Han, Y.H., Jun, B.H., Enhanced flux pinning and formation of $Ba_4Y_2CuMoO_y$ in top-seeded melt growth processed $YBa_2Cu_3O_{7-d}$ superconductors with Mo additions, *Supercond. Sci. Tech.*, 23 (12) (2010), 125009. https://doi.org/10.1088/0953-2048/23/12/125009

[7] Askerzade, I., Unconventional superconductors: anisotropy and multiband effects, Springer, 2012. https://doi.org/10.1007/978-3-642-22652-6

[8] Askerzade, I., Süperiletkenlik Fiziğine Giriş, Gazi Kitabevi, Ankara, 2005.

[9] Ozabaci, M., Contrasting effects of metal oxide dopants on the superconductivity of $YBa_2Cu_3O_{7-\delta}$ ceramics, *J. Mater. Sci.-Mater. El.*, 30 (2019), 20198-20204. https://doi.org/10.1007/s10854-019-02403-9

[10] Vovk, R.V., Khadzhai, G.Y., Dobrovolskiy, O.V., Incoherent charge transport induced by irradiation of YBCO single crystals with MeV electrons, *J. Mater. Sci.-Mater. El.*, 30 (2019), 4766-4769. https://doi.org/10.1007/s10854-019-00770-x

[11] Kabutoya, T., Koshimizu, M., Fujimoto, Y., Asai, K., X-ray Irradiation effects on the superconductive properties of $YBa_2Cu_3O_y$ and $GdBa_2Cu_3O_z$, *Sensor Mater.*, 29 (2017), 1465-1470. https://doi.org/10.18494/SAM.2017.1627

[12] Sueyoshi, T., Kotaki, T., Uraguchi, Y., Suenaga, M., Makihara, T., Fujiyoshi, T., Ishikawa, N., Flux pinning properties in YBCO films with growth-controlled nano-dots and heavy-ion irradiation defects, *Physica C*, 530 (2016), 72-75. http://dx.doi.org/10.1016/j.physc.2016.04.011

[13] Dadras, S., Falahati, S., Dehghani, S., Effects of graphene oxide doping on the structural and superconducting properties of $YBa_2Cu_3O_{7-\delta}$, *Physica C*, 548 (2018), 65-67. https://doi.org/10.1016/j.physc.2018.02.010

[14] Mahtali, M., Boudjema, E.H., Labbani, R., Chamekh, S., Bouabellou, Taoufik, A., Simon, C., Superconducting properties of YBaCuO ceramic doped with Ca and Zn^+, *Surf. Interface Anal.*, 42 (2010), 935-940 https://doi.org/10.1002/sia.3236

[15] Lazic, P., Pelc, D., Pozek, M., Despoja, V., Sunko, D.K., Effects of Sr and Zn doping on the metallicity and superconductivity of LSCO and YBCO, *J. Supercond. Nov. Magn.*, 28 (2015), 1299-1303. https://doi.org/10.1007/s10948-014-2909-1

[16] Savich, S.V., Samoylov, A.V., Kamchatnaya, S.N., Dobrovolskiy, O.V., Vovk, R.V., Solovjov, A.L., Omelchenko, L.V., Suppression of the order–disorder transition in Ti-doped YBaCuO compounds, *J. Mater. Sci.-Mater. El.*, 28 (2017), 11415-11419. https://doi.org/10.1007/s10854-017-6936-0

[17] Xu, Y., Suo, H.L., Yue, Z., Grivel, J.C., Liu, M., J_c enhancement by La-Al-O doping in Y-Ba-Cu-O films both in self-field and under magnetic field, *IEEE T. Appl. Supercon.*, 26 (3) (2016), 6602804. https://doi.org/10.1109/TASC.2016.2536805

[18] Sun, M., Liu, Z., Bai, C., Guo, Y., Lu, Y., Fan, F., Cai, C., Co-doping effects of Gd and Ag on YBCO films derived by metalorganic deposition, *Physica C*, 519 (2015), 47-52. http://dx.doi.org/10.1016/j.physc.2015.08.011

[19] Ai, X., Sun, A., Ma, L., Zhao, D., Zhang, Y., Luo, J., Co-doping effects of Ca and Ce on the superconducting properties in $Y_{1-x}Ca_x(Ba_{1-y}Ce_y)_2Cu_3O_{7-\delta}$, *J. Supercond. Nov. Magn.*, 25 (2012), 805-809. https://doi.org/10.1007/s10948-011-1349-4

[20] Slimani, Y., Hannachi. E., Salem, M.K.B., Hamrita, A., Varilci, A., Dachraoui, W., Ben Salem, M., Ben Azzouz, F., Comparative study of nano-sized particles $CoFe_2O_4$ effects on superconducting properties of Y-123 and Y-358, *Physica B*, 450 (2014), 7-15. http://dx.doi.org/10.1016/j.physb.2014.06.003

[21] Akyüz, G.B., Kocabaş, K., Yıldız, A., Özyüzer, L., Çiftçioğlu, M., The effects of Sb substitution on structural properties in $YBa_2Cu_3O_7$ superconductors, *J. Supercond. Nov. Magn.*, 24 (2011), 2189-2201. https://doi.org/10.1007/s10948-011-1180-y

[22] Moutalibi, N., M'chirgui, A., Noudem, J., Alumina nano-inclusions as effective flux pinning centers in Y–Ba–Cu–O superconductor fabricated by seeded infiltration and growth, *Physica C*, 470 (2010), 568-574. https://doi.org/10.1016/j.physc.2010.05.012

[23] Yeoh, W.K., Pathak, S.K., Shi, Y., Dennis, A.R., Cardwell, D.A., Babu, N.H., Strasik, M., Improved flux pinning in Y–Ba–Cu–O superconductors containing niobium oxide, *IEEE T. Appl. Supercon.*, 19 (3) (2009), 2970-2973. https://doi.org/10.1109/TASC.2009.2019131

[24] Tinkham, M., Resistive Transition of High-Temperature Superconductors, *Phys. Rev. Lett.*, 61 (14) (1988), 1658-1661. https://doi.org/10.1103/PhysRevLett.61.1658

[25] Inui, M., Littlewood, P.B., Coppersmith, S.N., Pinning and thermal fluctuations of a flux line in high-temperature superconductors, *Phys. Rev. Lett*., 63 (21) (1989), 2421-2424. https://doi.org/10.1103/PhysRevLett.63.2421

[26] Kandyel, E., Salem, A., Alqarni, A., Synthesis and characterization of doped $YBa_2Cu_4O_8$ superconductor by Cd^{+2}, *J. Supercond. Nov. Magn*., 26 (2013), 3363-3368. https://doi.org/10.1007/s10948-013-2199-z

[27] Delorme, F., Harnois, C., Monot-Laffez, I., Bismuth doping of top-seeding melt-texture-grown $YBa_2Cu_3O_{7-\delta}$ ceramics, *Supercond. Sci. Tech*., 16 (7) (2003), 739-747.

[28] Wimbush, S.C., Marx, W., Barth, A., Hall, S.R., On the incorporation of beryllium into the biotemplated synthesis of $YBa_2Cu_3O_{7-\delta}$, *Supercond. Sci. Tech*., 23 (9) (2010), 095003. https://doi.org/10.1088/0953-2048/23/9/095003

[29] Salem, M.K.B., Almessiere, M.A., Al-Otaibi, A.L., Salem, M.B., Azzouz, F.B., Effect of SiO_2 nano-particles and nano-wires on microstructure and pinning properties of $YBa_2Cu_3O_{7-d}$, *J. Alloy. Compd*., 657 (2016), 286-295. http://dx.doi.org/10.1016/j.jallcom.2015.10.077

[30] Jaroszynski, J., Hunte, F., Balicas, L., Jo, Y., Raicevic, I., Gurevich, A., Larbalestier, D.C., Balakirev, F.F., Fang, L., Cheng, P., Jia, Y., Wen, H.H., Upper critical fields and thermally-activated transport of $NdFeAsO_{0.7}F_{0.3}$ single crystal, *Phys. Rev. B*, 78 (2008), 174523. https://doi.org/10.1103/PhysRevB.78.174523

[31] Hamad, R.M., Kayed, T.S., Kunwar, S., Ziq, K.A., Thermally activated flux flow in $FeSe_{0.5}Te_{0.5}$ superconducting single crystal, *J. Phys. Conf. Ser*., 869 (2017), 012034. https://doi.org/10.1088/1742-6596/869/1/012034

[32] Anderson, P.W., Theory of flux creep in hard superconductors, *Phys. Rev. Lett*., 9 (7) (1962), 309-311. https://doi.org/10.1103/PhysRevLett.9.309

[33] Kim, Y.B., Hempstead, C.F., Strnad, A.R., Flux creep in hard superconductors, *Phys. Rev. Lett*., 131 (6) (1963), 2486-2495. https://doi.org/10.1103/PhysRev.131.2486

[34] Werthamer, N.R., Helfand, E., Hohenberg, P.C., Temperature and purity dependence of the superconducting critical field, H_{c2}. III. Electron Spin and Spin-Orbit Effects, *Phys. Rev*., 147 (1) (1966), 295-302. https://doi.org/10.1103/PhysRev.147.295

[35] Umakoshi, Y., Takahara. W., Hamada, K., Yamane, T., Effect of samarium and lanthanum substitution on the stability of superconductive properties of $YBa_2Cu_3O_x$, *J. Mater. Sci*., 26 (1991), 393-398.

[36] Çakır, B., Aydıner, A., Structural and magnetic properties of the ring shaped 40 wt% Y211 added TSMG Y123 bulk superconductors welded by Ag_2O added MPMG YBCO solder material, *J. Mater. Sci.-Mater. El*., 28 (2017), 17098-17106. https://doi.org/10.1007/s10854-017-7636-5

[37] Malik, B.A., Asokan, K., Ganesan, V., Singh, D., Malik, A.M., The magnetoresistance of YBCO/BZO composite superconductors, *Physica C*, 531 (2016), 85-92. http://dx.doi.org/10.1016/j.physc.2016.11.004